



## Article

# Doping of Graphene Nanostructure with Iron, Nickel and Zinc as Selective Detector for the Toxic Gas Removal: A Density Functional Theory Study

Fatemeh Mollaamin <sup>1,\*</sup>  and Majid Monajjemi <sup>2</sup>

<sup>1</sup> Department of Biomedical Engineering, Faculty of Engineering and Architecture, Kastamonu University, Kastamonu 37100, Turkey

<sup>2</sup> Department of Chemical Engineering, Central Tehran Branch, Islamic Azad University, Tehran 1496969191, Iran

\* Correspondence: smollaamin@gmail.com

**Abstract:** In this research, the ability of transition metals (TM)-doped graphene nanosheets to adsorb the toxic gas CO has been investigated. The Langmuir adsorption model was used, with a three-layered ONIOM, using the CAM-B3LYP functional accompanying the LANL2DZ and 6-31+G (d,p) basis sets, and using the Gaussian 16 revision C.01 program, on the complexes of CO adsorbed on (Fe, Ni, Zn)-doped graphene nanosheets. The order of the changes of charge density for the Langmuir adsorption of CO on Fe-doped, Ni-doped, and Zn-doped graphene nanosheets has been investigated. This shows the greatest change of charge density for the Ni-doped graphene nanosheet. However, based on NMR spectroscopy, sharp peaks around the Ni-doped area on the surface of the graphene nanosheet have been observed. In addition, the Ni-doped graphene nanosheet has a large effect on the bond orbitals of C-Ni in the adsorption of CO, having the maximum occupancy. The values of  $\Delta G_{ads}^0$ , calculated through IR, showed that  $\Delta G_{ads,CO \rightarrow Fe-doped GR}^0$  has the highest value, because of a charge density transfer from the oxygen atom in carbon monoxide to the Fe-doped graphene nanosheet. The frontier molecular orbitals, HOMO and LUMO, and the band energy gap accompanying some chemical reactivity parameters, have revealed the attributes of the molecular electrical transport of (Fe, Ni, Zn)-doped graphene nanosheets for the adsorption of CO. As a result, since a CO molecule interacts simultaneously with a Fe, Ni, or Zn atom and the C-C nanosheet, at first it might be separated, as in this state a CO atom constructs a physical bond with the Fe, Ni, or Zn atom, and then the other could be adsorbed chemically on the C-C nanosheet surface. Finally, our results have shown that a considerable amount of charge transfer occurs between CO molecules and TM-doped graphene nanosheets after adsorption, which suggests that TM-doped graphene is more sensitive and selective to the adsorption of CO than a pristine graphene surface.



**Citation:** Mollaamin, F.; Monajjemi, M. Doping of Graphene Nanostructure with Iron, Nickel and Zinc as Selective Detector for the Toxic Gas Removal: A Density Functional Theory Study. *C* **2023**, *9*, 20. <https://doi.org/10.3390/c9010020>

Academic Editors: Sergey Mikhalovsky and Rosa Busquets

Received: 12 January 2023

Revised: 7 February 2023

Accepted: 8 February 2023

Published: 9 February 2023



**Copyright:** © 2023 by the authors. Licensee MDPI, Basel, Switzerland. This article is an open access article distributed under the terms and conditions of the Creative Commons Attribution (CC BY) license (<https://creativecommons.org/licenses/by/4.0/>).

**Keywords:** (Fe, Ni, Zn)-doped/GSs; CO; toxic gases; ONIOM/DFT; NMR; IR; UV-VIS; HOMO; LUMO

## 1. Introduction

Discovering and controlling air polluting gases like carbon monoxide (CO) is essential, because this gas is toxic and damages the environment and the health of people [1–3].

Graphene-based materials which have been doped with transition metals can be used as toxic gas sensors [4–9].

There are different practical applications of carbon nanostructures, such as hydrogen adsorption, pollutant molecules adsorption, gas sensor devices, etc. [10–18]

The most significant and newest research in this field relates to the adsorption of pollutants or hazardous gases by applying carbon nanostructures [19–22].

Among the most studied pollutant gases are carbon monoxide, carbon dioxide, methanol, methane, nitrogen monoxide, nitrogen dioxide, ozone, and formaldehyde, etc.

Sensing and sampling toxic and harmful gases like CO, CO<sub>2</sub>, NO, N<sub>2</sub>O, CH<sub>4</sub>, SO<sub>2</sub>, and H<sub>2</sub>S can largely help to maintain human health and ecosystems [23–26].

Recently, the development of catalysts with a high resistance to chlorine, for volatile organic compound (VOC) degradation, has been considered for removing air pollution [27]. Moreover, researchers have used DFT calculations to show that alkali metals and H<sub>2</sub>O are appropriate for the adsorption of benzyl alcohol, benzaldehyde, benzoic acid, toluene, and O<sub>2</sub> gases, which represent new opinions for increasing the yields of system and water promotion in manganese-based compounds of for VOC monitoring [28]. Another investigation has illustrated the efficiency of a meso-Pt/CeO<sub>2</sub> catalyst, derived from a synthesized Pt/Ce-MOF, for adsorbing O<sub>2</sub> and CO<sub>2</sub> in the air, and other principal intermediate products containing toluene, benzyl alcohol, benzoic acid, benzoate, maleic anhydride, and water [29].

These days, many materials, such as carbon based materials, have been investigated and applied for the adsorptive removal of toxic gases [30–32]. Therefore, it is essential to make highly sensitive gas sensors for detecting toxic gases. Therefore, the remarkable surfaces of carbon nanostructures can be an important factor for gas sensing and gas adsorption devices. In addition, the doping of these compounds with transition metals might enhance their adsorption ability, and adjust their selective adsorption as the excellent dopant applicants. It seems that donor or acceptor molecules on graphene can considerably alter the electronic properties through first-principles methods [33].

Carbon monoxide (CO), as a hazardous gas, is an essential compound in environmental pollutants, which has been investigated in several studies through adsorption on graphene (GR), consisting of pristine graphene, nitrogen-doped graphene, and metal-doped graphene by first-principles studies [34].

Thus, for improving the sensitivity toward adsorbing the gases by graphene, doping can be a good method. In this article, we have applied a first-principles simulation of the interactions between carbon monoxide molecules and graphene nanosheets doped with various transition metals (Fe, Ni, Zn).

## 2. Materials, Modeling and Computational Details

### 2.1. Adsorptive Removal of Toxic Gases

A range of experimental investigations have concentrated on the gas adsorption susceptibilities of single-walled carbon nanotubes (SWCNTs) and multiple walled carbon nanotubes (MWCNTs), showing a good accord with the Langmuir adsorption system. The key factor making nanostructures suitable for use as gas sensors is the charge transfer between the adsorbent (nanosurface) and the adsorbate (gas molecule), due to the effects of the carbon nanostructure network [35]. Graphene has been frequently applied as an absorptive surface for the adsorption of CO, CO<sub>2</sub>, NO, NO<sub>2</sub>, NH<sub>3</sub>, and H<sub>2</sub>O, as prospected through density functional theory calculations. The impressive capture of damaging chemicals is of major importance both for the conservation of the environment and for those who are at danger of being exposed to such materials. The application of graphene nanosheets with an adequate size and shape is not enough for the efficient capture of toxic gases, and other more specific substances between the hazardous adsorbates and the host are required. The existence of metal sites on the pure surface might increase the adsorption selectivity/efficiency of graphene towards certain toxic compounds via coordination bonds or  $\pi$ -complex interactions. TM-doped graphene has been noted as a possible applicant to distinguish various polluting gases which interact poorly with pure graphene [36–39].

### 2.2. Langmuir Adsorption Model & Charge Density Analysis

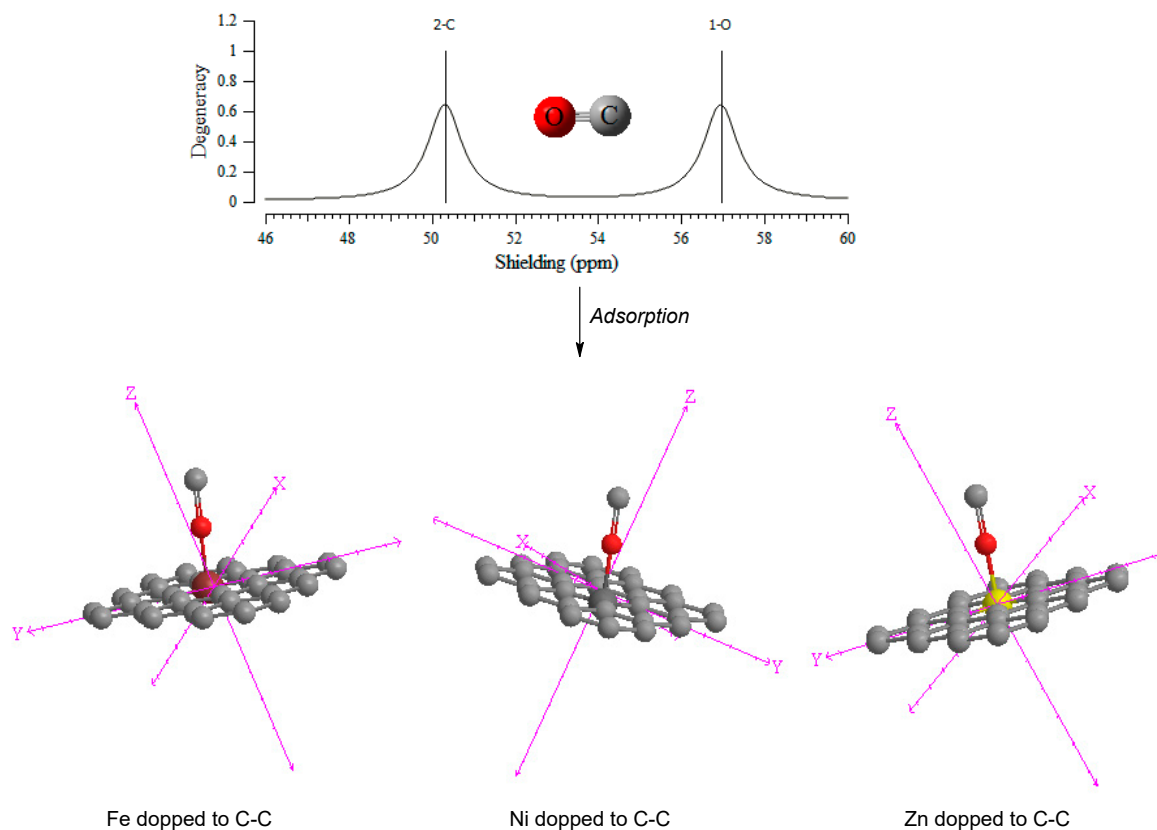
Langmuir adsorption can be defined as a physico-chemical interaction on the surface of a homogeneous solid material that adsorbs compounds without any interactions with each other, making a mono layer of molecules on the surface of the solid state.

The Langmuir adsorption equation is the following [40]:

$$\theta_A = \frac{V}{V_m} = \frac{K_{eq}^A p_A}{1 + K_{eq}^A p_A} \quad (1)$$

where  $\theta_A$  is the fractional occupancy of the adsorption sites; the ratio of  $V$ , the volume of gas adsorbed onto the solid, to  $V_m$ , the volume of the gas molecules monolayer coating the entire surface of the solid and totally filled by the adsorbate. A continuous monolayer of adsorbate molecules coating a homogeneous solid surface is the conceptual basis for this adsorption system [41,42].

Different studies have concentrated on the gas adsorption susceptibilities of carbon nanosurfaces which show a good agreement with the Langmuir adsorption model. The adsorption of toxic CO gas on Fe-doped, Ni-doped, and Zn-doped graphene nanosheets has been assigned by the most suitable Langmuir isotherm, which exhibits the chemisorptive nature of the bond between  $:C\equiv O:$  molecules and a TM-doped graphene nanosheet, the equilibrium electron distribution of the adsorbing compound between the solid and gas phases, and a monolayer attribute. The adsorbed  $:C\equiv O:$  molecules are kept on the TM-doped graphene nanosheet by Langmuir chemisorption (Scheme 1).



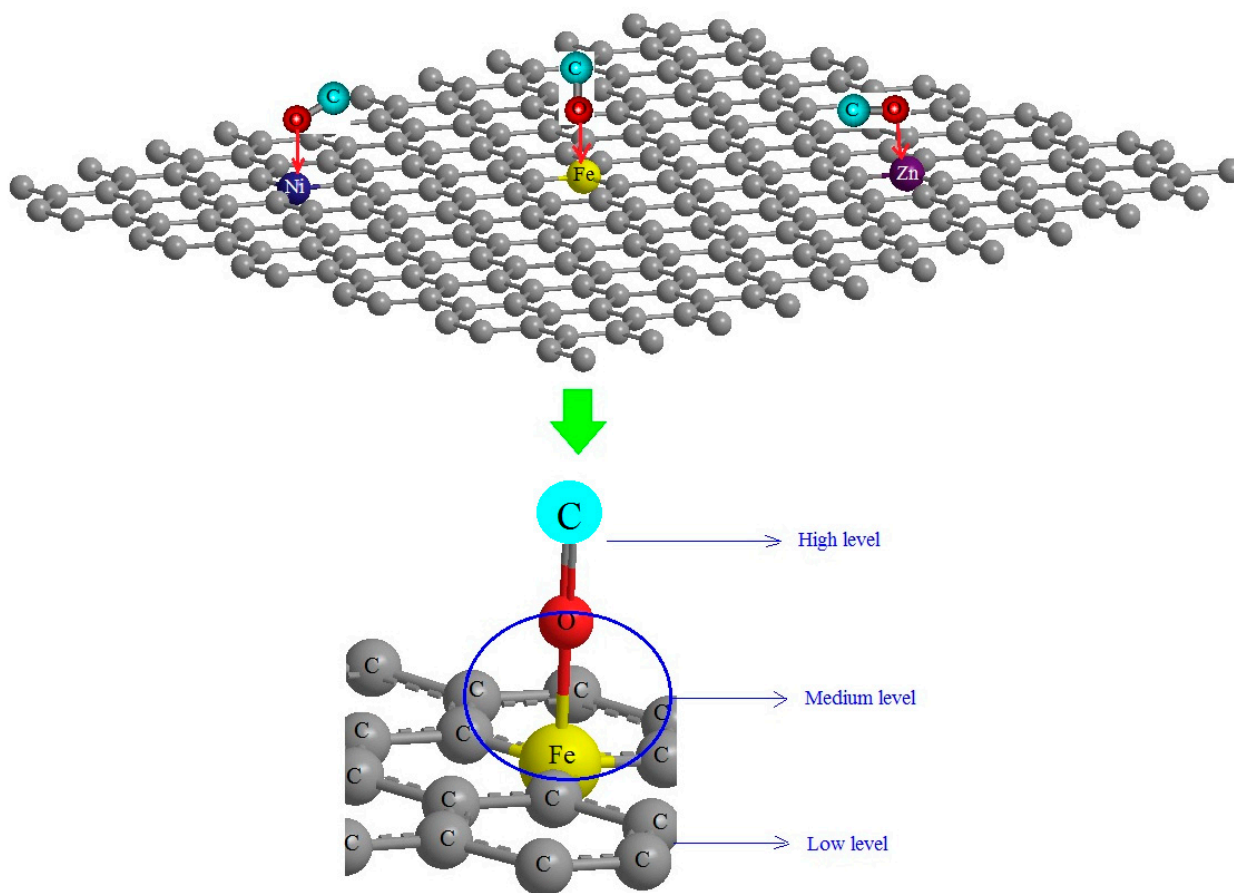
**Scheme 1.** NMR spectrum of  $:C\equiv O:$  gas molecules which are adsorbed on Fe-doped, Ni-doped, and Zn-doped graphene nanosheets.

In fact, the nature of the gas sensing mechanism in the TM (Fe, Ni, Zn)-doped graphene nanosheets is due to charge transfer between the surface and the adsorbed CO molecules. An analysis of the changes of charge density during the adsorption process has illustrated that Fe-doped, Ni-doped, and Zn-doped graphene nanosheets show Mulliken charges of  $-1.345$ ,  $-2.087$ ,  $-1.416$ , respectively, before the adsorption of carbon monoxide, and  $-1.833$ ,  $-1.726$ ,  $-1.424$ , respectively, after the adsorption of carbon monoxide. Therefore, the changes of charge density for the Langmuir adsorption of carbon monoxide on Fe-doped, Ni-doped, and Zn-doped graphene nanosheets, respectively, are

$\Delta Q_{\text{Ni-doped}} = +2.087(e) \gg \Delta Q_{\text{Zn-doped}} = -0.008(e) \gg \Delta Q_{\text{Fe-doped}} = -0.488(e)$ . The values of the changes of charge density illustrate an appropriate selectivity for the Ni-doped graphene nanosheet compared to the Fe-doped and Zn-doped graphene nanosheets, due to a more significant charge transfer.

### 2.3. ONIOM by Density Functional Theory

The combination of three levels of theory, in decreasing order of accuracy, has been defined including high, medium, and low levels, using the ONIOM method (Scheme 2). The high-level has been performed using the DFT method of CAM-B3LYP LANL2DZ for iron, nickel, zinc-doped graphene nanosheets, and using 6-31+G (d,p) for the adsorbate molecule. The medium-level has used semi-empirical methods in the adsorption site.



**Scheme 2.** The mechanism of the Langmuir adsorption of CO onto TM (Fe, Ni, Zn)-doped graphene nanosheets based on optimized coordination using the three-layered ONIOM method.

The applied semi-empirical method in the medium-level is PM3, which was proposed by Stewart in 1989 [43]. The PM3 method employs two Gaussian functions for the core repulsion function, and the numerical values of the various factors. Moreover, it takes some of the parameters' values from optimization.

Finally, a low-level has been performed on the graphene nanosheet (adsorbent) with MM2 force fields,  $E_{\text{ONIOM}} = E_{\text{High}} + E_{\text{Medium}} + E_{\text{Low}}$ , (Scheme 2) [44].

On the other hand, the three-layered method of ONIOM allows us to discover a larger system, more exactly than the one-layered model, which could treat a medium-sized system precisely like a ground system with an acceptable accuracy [45].

In this article, the structures have been calculated, using density functional theory (DFT), on the mechanisms of adsorption of CO by TM (Fe, Ni, Zn)-doped graphene nanosheets through bonding between the transition metals Fe, Ni, and Zn, and the gas molecule ( $:\text{C}\equiv\text{O}:$ ). It has been found that the surface binding site preference of the O-atom

of CO is largely affected by the presence of neighboring atoms in the graphene sheet. The calculated CO→ Fe-doped/Gr, CO→ Ni-doped/Gr, and CO→ Zn-doped/Gr pair distribution functions have indicated that the formation of clusters directs to shorter O→Fe, O→Ni and O→Zn bond lengths when compared to homogeneous growth (Scheme 2).

DFT, or density functional theory, approaches are the standard and the most employed theoretical methods for electronic structure calculations [46–50]. The appearance of the generalized gradient approximation (GGA) for the exchange–correlation functional increased the DFT accuracy [51], and the predicted molecular structures, relative energies, and frequencies are nearly analogous to the second order Møller–Plesset perturbation theory (MP2) method, with notable success in predicting the behavior of transition metal clusters [52]. The Hohenberg–Kohn (HK) functions have made the electronic density admissible as a basic variable for electronic and structure calculations. On the other hand, progress on practical DFT approaches only became remarkable after W. Kohn and L. J. Sham published their famous set of equations, which are represented as the Kohn–Sham (KS) equations [53,54].

Hybrid functional is a group of approximations for the exchange–correlation energy functional in DFT (Density Functional Theory), which combines a part of the exact exchange from the HF (Hartree–Fock theory) method with the rest of the exchange–correlation energy from other information, such as empirical or ab initio methodologies. Therefore, the exact exchange energy functional is illustrated by the Kohn–Sham orbitals instead of the density, so is placed as the indirect density functional. This study has applied the influence of the hybrid functional of the three-parameter basis set of B3LYP (Becke, Lee, Yang, Parr), within the framework of DFT, upon theoretical calculations [55,56]. Using the electronic density within the KS figure allows for a significant decrease of the computational request of quantum calculations. Therefore, the KS approach simplifies the path for investigating systems that cannot be studied by conventional ab initio systems. Kohn and Sham presented a solution which used mono-electronic orbitals to estimate the kinetic energy in a simple and approximately precise way, by leaving a residual correction that can be calculated separately. Therefore, one begins with a reference system of  $M$  non-interacting electrons subjected to the external potential  $v_s$  and with a Hamiltonian [53,54]:

$$\hat{H}_s = -\sum_i^M \frac{1}{2} \nabla_i^2 + \sum_i^M v_s(\vec{r}_i) = \sum_i^M \hat{h}_{si}; \hat{h}_s = -\frac{1}{2} \nabla_i^2 + v_s(\vec{r}_i) \quad (2)$$

By introducing the single particle orbitals  $\psi_i$ , all electronic densities physically acceptable for the system of non-interacting electrons can be written in the form:

$$\rho(\vec{r}) = \sum_i^M |\psi_i(\vec{r})|^2 \quad (3)$$

Finally, the total energy can be calculated by the KS method through the following equation:

$$E[\rho] = \sum_i^M n_i \langle \psi_i | \left[ -\frac{1}{2} \nabla^2 + v_{ext}(\vec{r}) + \frac{1}{2} \int \frac{\rho(\vec{r}')}{|\vec{r} - \vec{r}'|} d\vec{r}' \right] | \psi_i \rangle + E_{xc}[\rho] + \frac{1}{2} \sum_{\beta}^N \sum_{\alpha \neq \beta}^N \frac{Z_{\alpha} Z_{\beta}}{|\vec{R}_{\alpha} - \vec{R}_{\beta}|} \quad (4)$$

So, the exact exchange energy functional is illustrated by the Kohn–Sham orbitals instead of the density, so is placed as the indirect density functional. This study has applied the influence of the hybrid functional of the three-parameter basis set of B3LYP (Becke, Lee, Yang, Parr) within the framework of DFT upon theoretical calculations [55,56]. The popular B3LYP (Becke, three-parameter, Lee–Yang–Parr) exchange–correlation functional is [57–59]:

$$E_{XC}^{B3LYP} = (1 - \alpha) E_X^{LSDA} + \alpha E_X^{HF} + b \Delta E_X^B + (1 - c) E_C^{LSDA} + c E_C^{LYP} \quad (5)$$



where  $\alpha = 0.20$ ,  $b = 0.72$ ,  $c = 0.81$  is a generalized gradient approximation: the Becke exchange functional [55] and the correlation functional of Lee, Yang and Parr [56] for B3LYP and  $E_c^{LSDA}$  is the VWN local spin density approximation to the correlation functional [60].

Transition metal-doped graphene sheets have been built by a rigid system and Z-Matrix format, of which a blank line has been placed, and after that the following information has been illustrated. The rigid PES has been performed at the CAM-B3LYP functional level [61], and employing the LANL2DZ/6-31+G (d,p) basis sets to assign HOMO, LUMO, Mulliken charges, nuclear magnetic resonance properties, dipole moment, thermodynamic characteristics, and other quantum properties, for this study [62] of CO adsorbed onto TM-doped graphene nanosheets including CO  $\rightarrow$  Fe-doped/Gr, CO  $\rightarrow$  Ni-doped/Gr, and CO  $\rightarrow$  Zn-doped/Gr using the Gaussian 16 program package [63].

### 3. Results

In this investigation, the transition metals, iron, nickel, and zinc, doped on the graphene nanosheets, have been investigated as efficient surfaces for the adsorption of the toxic gas, carbon monoxide, which causes air pollution. These experiments have been accomplished using spectroscopy analysis of some physical and chemical properties.

#### 3.1. NMR Spectroscopy & NBO Analysis

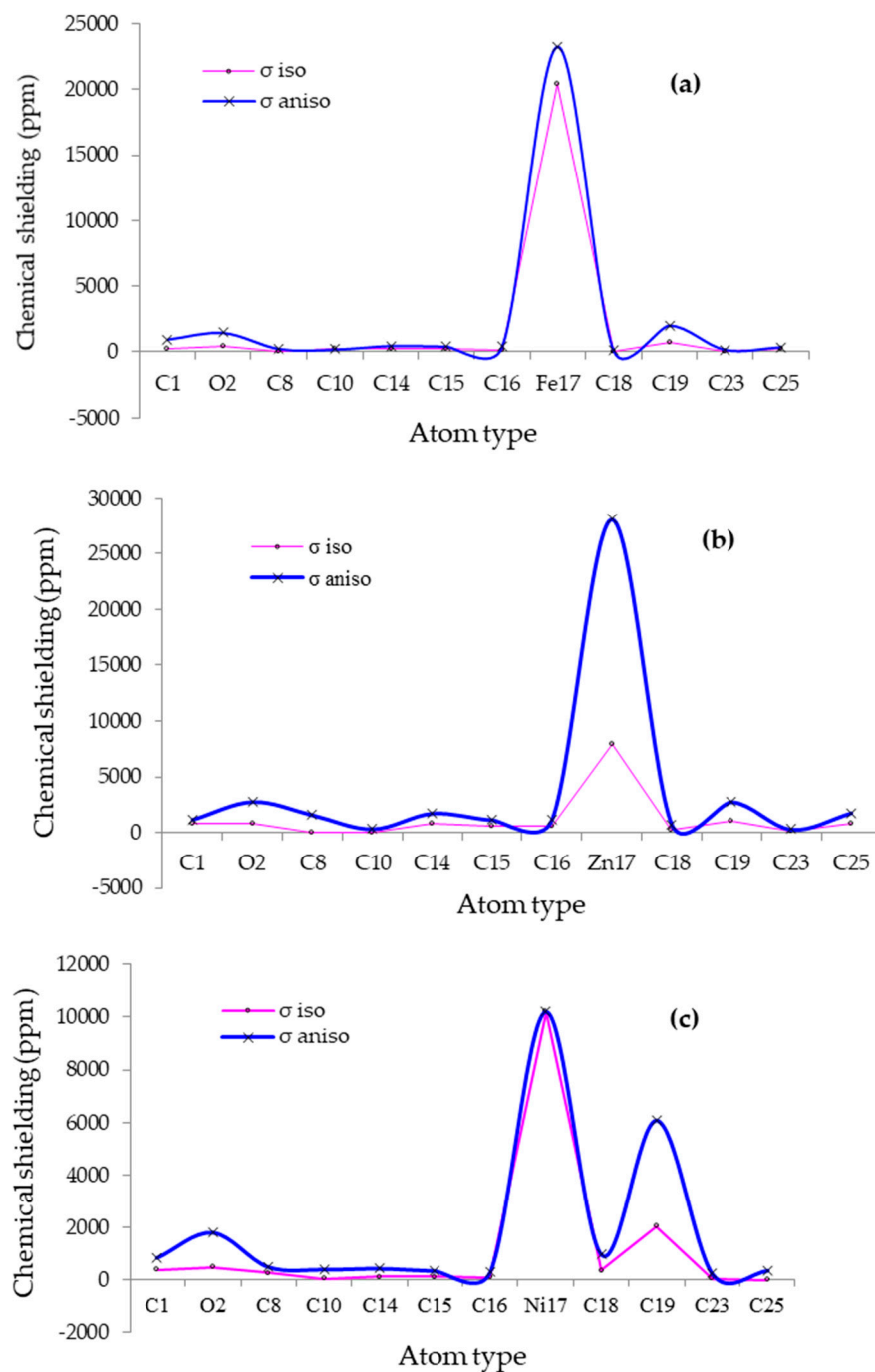
Isotropic ( $\sigma_{iso}$ ) and anisotropy ( $\sigma_{aniso}$ ) shielding tensors of NMR spectroscopy for certain atoms in the active site of CO adsorption on the Fe, Ni, Zn-doped graphene (Gr) nanosheets, through the formation of the bindings between the gas molecules and the solid surface, have been calculated using the Gaussian 16 program software [63] and are reported in Table 1.

**Table 1.** Calculated NMR chemical shielding tensors for some atoms in the active site of CO gas adsorption on the TM (Fe, Ni, Zn)-doped/Gr nanosheets.

CO $\rightarrow$ Fe-Doped/Gr			CO $\rightarrow$ Ni-Doped/Gr			CO $\rightarrow$ Zn-Doped/Gr		
Atom	$\sigma_{iso}$	$\sigma_{aniso}$	Atom	$\sigma_{iso}$	$\sigma_{aniso}$	Atom	$\sigma_{iso}$	$\sigma_{aniso}$
C1	233.4257	968.2802	C1	382.6002	844.5628	C1	817.8193	1200.6025
O2	394.9638	1463.9175	O2	495.3022	1809.7355	O2	788.7503	2796.0869
C8	29.2897	240.5192	C8	260.1665	501.7185	C8	11.2789	1596.7923
C10	204.8650	198.5053	C10	48.3307	404.4537	C10	48.7486	342.4682
C14	235.1941	480.5288	C14	113.4488	438.0594	C14	780.6997	1754.9402
C15	247.1604	421.2191	C15	111.3020	348.6676	C15	562.6576	1162.1428
C16	166.2217	406.5082	C16	104.6419	310.2320	C16	576.8997	1196.7425
Fe17	20,464.6572	23,260.8181	Ni17	10,207.7265	10,207.7265	Zn17	7974.7632	28,112.8322
C18	38.1089	134.3989	C18	362.1582	967.9775	C18	244.7286	749.2167
C19	752.6628	2028.2108	C19	2042.4580	6083.9999	C19	1100.1399	2780.5764
C23	89.6758	183.7640	C23	58.0015	232.5619	C23	177.0834	302.6073
C25	269.0681	379.3128	C25	3.1888	359.3453	C25	834.3115	1785.4044

Chemical shielding (CS) tensors in principal axes system evaluate the isotropic chemical-shielding ( $\sigma_{iso}$ ), anisotropic chemical-shielding ( $\sigma_{aniso}$ ) [64]:  $\sigma_{iso} = \frac{\sigma_{33} + \sigma_{22} + \sigma_{11}}{3}$ ;  $\sigma_{aniso} = \sigma_{33} - \frac{\sigma_{22} + \sigma_{11}}{2}$

In Figure 1, the degeneracy of NMR graphs versus chemical shielding (ppm) is shown for CO adsorbed onto the Fe-doped/Gr, Ni-doped/Gr, Zn-doped/Gr nanosheets.



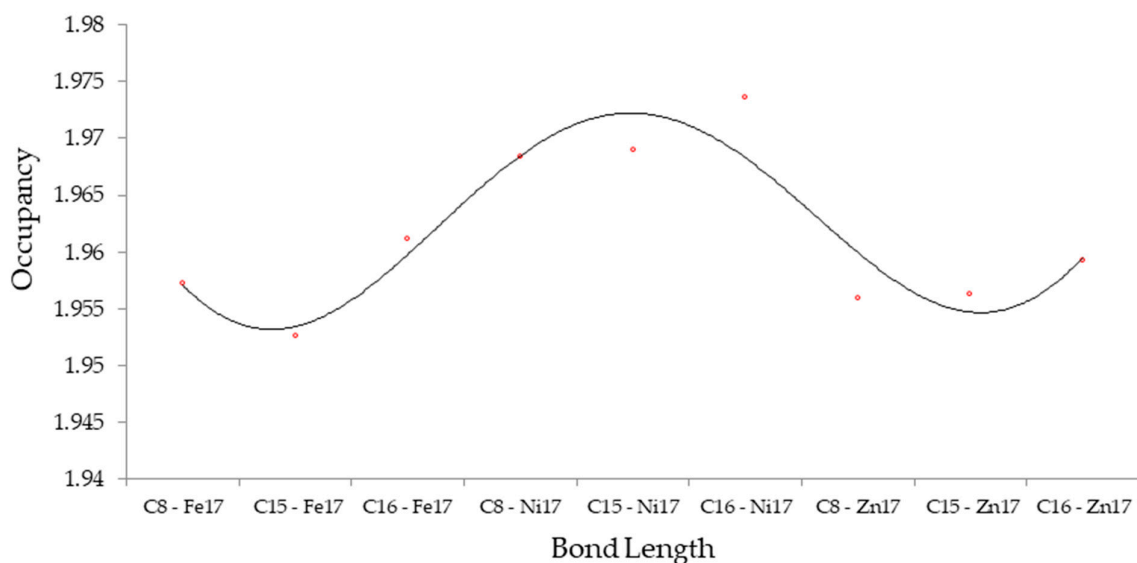
**Figure 1.** NMR spectroscopy for the adsorption of CO on the (a) Fe-doped/Gr, (b) Ni-doped/Gr, and (c) Zn-doped/Gr nanosheets.

The graphs of NMR spectroscopy in Figure 1a,b show approximately identical chemical shielding behaviors of the isotropic and anisotropy parameters for the Fe-doped/Gr, and Zn-doped/Gr nanosheets, with a sharp peak close to the Fe-doped and Zn-doped areas on the surface of graphene, respectively. However, two sharp peaks are observed around the Ni-doped surface of graphene and C19, in the region of the junction between O<sub>2</sub> and Ni17 (Figure 1c).

Furthermore, a Natural Bond Orbital (NBO) analysis of carbon monoxide (CO) adsorbed on the TM (Fe, Ni, Zn)-doped graphene (Gr) nanosheets has illustrated the character of electronic conjugation between bonds in the gas molecules and TM-doped/Gr nanosheets (Table 2 and Figure 2).

**Table 2.** NBO analysis for CO on the TM (Fe, Ni, Zn)-doped/Gr nanosheets.

CO → TM-Doped/Gr Nanosheet	Bond Orbital	Occupancy	Hybrids
CO → Fe-doped/Gr	BD (1) C8–Fe17	1.95721	0.8066 (sp <sup>1.69</sup> ) C + 0.5910 (sp <sup>0.31</sup> d <sup>3.07</sup> ) Fe
	BD (1) C15–Fe17	1.95267	0.8154 (sp <sup>1.40</sup> ) C + 0.5789 (sp <sup>0.34</sup> d <sup>3.23</sup> ) Fe
	BD (1) C16–Fe17	1.96117	0.8180 (sp <sup>1.46</sup> ) C + 0.5753 (sp <sup>0.40</sup> d <sup>4.30</sup> ) Fe
CO → Ni-doped/Gr	BD (1) C8–Ni17	1.96844	0.8015 (sp <sup>1.59</sup> ) C + 0.5980 (sp <sup>0.34</sup> d <sup>2.00</sup> ) Ni
	BD (1) C15–Ni17	1.96893	0.8094 (sp <sup>1.39</sup> ) C + 0.5872 (sp <sup>0.38</sup> d <sup>2.24</sup> ) Ni
	BD (1) C16–Ni17	1.97360	0.8191 (sp <sup>1.04</sup> ) C + 0.5737 (sp <sup>0.58</sup> d <sup>4.28</sup> ) Ni
CO → Zn-doped/Gr	BD (1) C8–Zn17	1.95595	0.8224 (sp <sup>1.45</sup> ) C + 0.5689 (sp <sup>2.02</sup> d <sup>0.43</sup> ) Zn
	BD (1) C15–Zn17	1.95624	0.8055 (sp <sup>1.33</sup> ) C + 0.5926 (sp <sup>1.39</sup> d <sup>1.08</sup> ) Zn
	BD (1) C16–Zn17	1.95929	0.8052 (sp <sup>1.35</sup> ) C + 0.5930 (sp <sup>1.44</sup> d <sup>1.27</sup> ) Zn

**Figure 2.** Occupancy fluctuation extracted from the NBO method for bond lengths of C-Fe, C-Ni and C-Zn through adsorption of CO on the TM (Fe, Ni, Zn)-doped/Gr nanosheets.

In Figure 2, fluctuations are observed in the occupancies of the natural bond orbitals for the CO → Fe-doped, CO → Fe-doped, and CO → Fe-doped graphene nanosheets through the Langmuir adsorption process, indicating that the active oxygen atom in carbon monoxide is close to the nanosheet's surface. The bond orbitals of C8–Ni17, C15–Ni17, and C16–Ni17 in the adsorption of CO in the Ni-doped/Gr, show the maximum occupancy.

### 3.2. Thermodynamic Properties & IR Spectroscopy Analysis

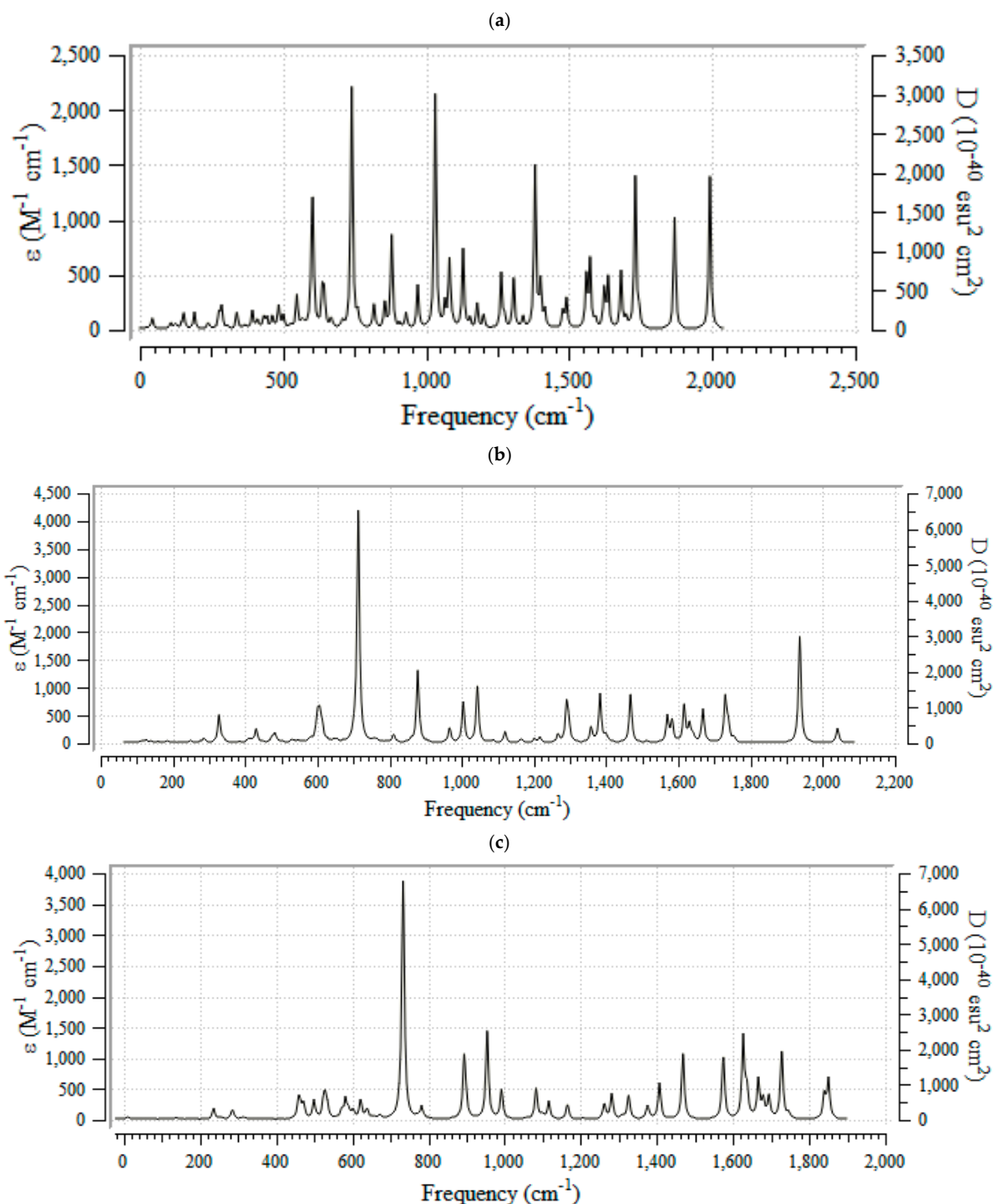
Thermodynamic parameters have been estimated for the adsorption of toxic carbon monoxide (:C≡O:) on the surfaces of (Fe, Ni, Zn)-doped graphene nanosheets as gas sensors which can be used as selective detectors for toxic gases (Table 3).

**Table 3.** The physico-chemical properties of CO adsorbed on Fe-, Ni-, and Zn-doped graphene nanosheets as selective gas sensors.

Compound	$\Delta H^\circ \times 10^{-4}$ (kcal/mol)	$\Delta G^\circ \times 10^{-4}$ (kcal/mol)	S <sup>o</sup> (Cal/K.mol)	Dipole Moment (Debye)
Fe-C	−146.2782	−146.2816	111.175	2.3199
Ni-C	−162.4793	−162.4828	116.150	13.6226
Zn-C	−178.2030	−178.2066	120.533	1.7301
:C≡O:	−69.784	−69.798	47.100	0.2373
:C≡O:→Fe-C	−153.2461	−153.2501	131.502	14.2253
:C≡O:→Ni-C	−168.3894	−168.3930	119.303	12.8804
:C≡O:→Zn-C	−185.1696	−185.1733	123.534	8.6863

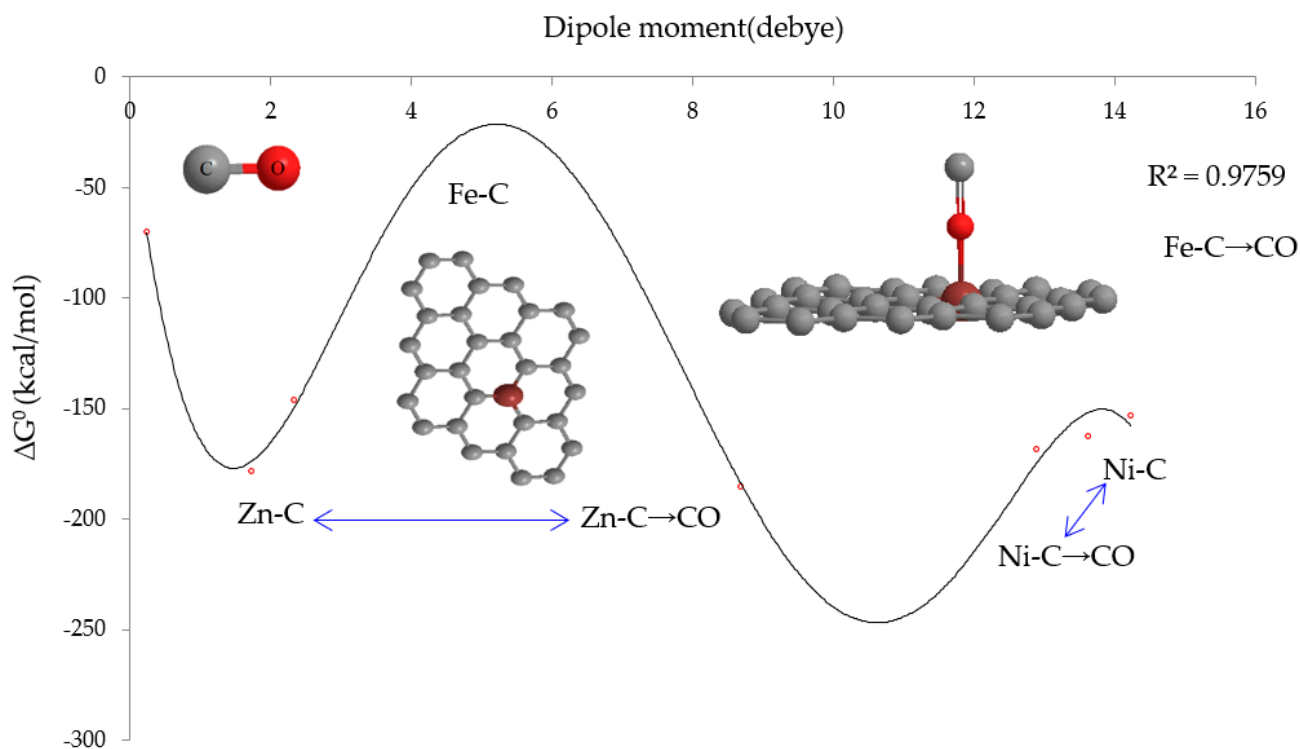


Moreover, the infrared spectra for the adsorption of CO by Fe-doped, Ni-doped, and Zn-doped graphene nanosheets are shown in Figure 3a–c. Each of these spectra cover the approximate frequency range 500–2000  $\text{cm}^{-1}$ , with the complexes of  $:\text{C}\equiv\text{O} \rightarrow \text{Fe-C}$ ,  $:\text{C}\equiv\text{O} \rightarrow \text{Ni-C}$ ,  $:\text{C}\equiv\text{O} \rightarrow \text{Zn-C}$  having the strongest peaks approximately at 750  $\text{cm}^{-1}$ . Figure 3a shows the strongest peaks for the  $:\text{C}\equiv\text{O} \rightarrow \text{Fe-C}$  graphene nanosheet at 600  $\text{cm}^{-1}$ , 750  $\text{cm}^{-1}$ , 875  $\text{cm}^{-1}$ , 1050  $\text{cm}^{-1}$ , 1375  $\text{cm}^{-1}$ , 1725  $\text{cm}^{-1}$ , 1850  $\text{cm}^{-1}$ , and 2000  $\text{cm}^{-1}$ . It is seen in Figure 3b,c that the strongest peak in the IR spectra for the  $:\text{C}\equiv\text{O} \rightarrow \text{Ni-C}$  and  $:\text{C}\equiv\text{O} \rightarrow \text{Zn-C}$  graphene nanosheets is at roughly 750  $\text{cm}^{-1}$ .



**Figure 3.** Changes of frequency ( $\text{cm}^{-1}$ ) in the IR spectra for (a) Fe-, (b) Ni-, (c) Zn-doped graphene nanosheets as selective gas sensors.

In Figure 4, it is seen that the maximum of the Langmuir adsorption isotherm plots based on  $\Delta G_{ads}^0$  versus dipole moment may depend on the interactions between the CO and the TM-doped graphene nanosheets. The order of the Gibbs free energy changes for showing the selectivity of the TM-doped graphene nanosheets is  $\Delta G_{CO \rightarrow Zn-C}^0 > \Delta G_{CO \rightarrow Ni-C}^0 > \Delta G_{CO \rightarrow Fe-C}^0$  (Figure 4).



**Figure 4.** The changes of Gibbs free energy for the adsorption of CO as a toxic gas on TM (Fe, Ni, Zn)-doped graphene nanosheets.

For calculating the adsorption's Gibbs free energy, the total energy of an isolated CO molecule should be measured. Therefore, a graphene nanosheet doped with Fe, Ni, and Zn was modeled with a single CO molecule adsorbed on it, and then the CAM-DFT calculation was implemented with the same force and energy convergence precision as the adsorption systems. The adsorptive capacity of CO on the TM-doped graphene nanosheets is described by the  $\Delta G_{ads}^0$  amounts.


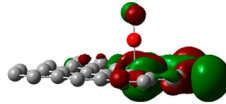
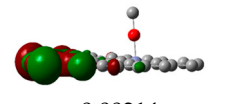
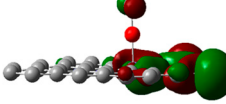
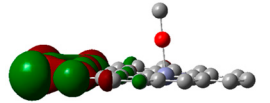
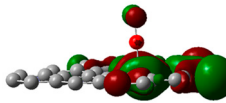
$$\Delta G_{ads}^0 = \Delta G_{CO \rightarrow TM-C}^0 - (\Delta G_{CO}^0 + \Delta G_{TM-C}^0); TM = Fe, Ni, Zn \quad (6)$$

On the basis of the data in Table 3, it is predicted that the adsorption of CO on the TM-doped graphene nanosheets might be physical and chemical in nature. As shown in Figure 4, all the computed  $\Delta G_{ads}^0$  amounts are very similar, which demonstrates the agreement of the evaluated data by all methods, and the validity of the calculations.

### 3.3. Frontier Molecular Orbital Analysis and Ultraviolet & Visible Spectroscopy

The frontier molecular orbital of HOMO energy is created using ionization, and the frontier molecular orbital of LUMO energy is seen due to the electron cohesion. These factors were estimated and reported for the adsorption of the pollutant gas on the TM (Fe, Ni, Zn)-doped graphene nanosheets, in Table 4. The band energy gap accompanying HOMO and LUMO energies indicates the pictorial illustration of the frontier molecular orbital and their related total values that are magnificent factors for exploring the molecular characteristics of capable structures in adsorption of CO on the TM-doped graphene nanosheet (Table 4).

**Table 4.** The LUMO (a.u.), HOMO (a.u.), band energy gap ( $\Delta E$ /eV) and other parameters (eV) for adsorption of CO as a toxic gas on TM (Fe, Ni, Zn)-doped graphene nanosheets, using CAM-B3LYP/LANL2DZ, 6-31+G (d,p).

Gas $\rightarrow$ TM-Doped Gr@NS	LUMO	HOMO	$\Delta E$	$\mu$	$\chi$	$\eta$	$\zeta$	$\psi$
CO $\rightarrow$ Fe-C	 −0.00480	 −0.12195	3.1878	−1.7245	1.7245	1.5939	0.3137	0.9329
CO $\rightarrow$ Ni-C	 −0.00314	 −0.13644	3.6272	−1.8991	1.8991	1.8136	0.2757	0.9943
CO $\rightarrow$ Zn-C	 −0.00907	 −0.15289	3.9135	−2.2035	2.2035	1.9567	0.2555	1.2407

$\Delta E = E_{\text{LUMO}} - E_{\text{HOMO}}$ ;  $\mu = (E_{\text{HOMO}} + E_{\text{LUMO}})/2$ ;  $\chi = -(E_{\text{HOMO}} + E_{\text{LUMO}})/2$ ;  $\eta = (E_{\text{LUMO}} - E_{\text{HOMO}})/2$ ;  $\zeta = 1/(2\eta)$ ;  $\psi = \mu^2/(2\eta)$

Furthermore, for achieving a more efficient approving in distinguishing the structural properties of the adsorption complexes of  $\text{CO} \rightarrow \text{TM}$  (Fe, Ni, Zn)-doped graphene nanosheets, a group of chemical reaction factors (Table 4) [65–67].

In fact, the HOMO represents the ability to donate an electron, and the LUMO as an electron acceptor, indicates the susceptibility of accepting an electron. So, the energy gap ( $\Delta E = E_{\text{LUMO}} - E_{\text{HOMO}}$ ) exhibits the diversity of energy between the LUMO and HOMO orbitals, representing the strength of the compound, and introduce the chemical function of the structure. In this investigation, the energy gap shows how the toxic gas CO can be adsorbed on the TM (Fe, Ni, Zn)-doped graphene nanosheets, using the B3LYP/LANL2DZ, 6-311+G (2d, p) computational approach. In addition, the frontier orbitals manage a crucial step in the optical and electrical parameters, such as the ultraviolet-visible spectrum [68]. The energy gap between the LUMO and HOMO determines the likelihood of molecular electrical transfer [69]. Using Frank–Condon theory, the most value of absorption relates to an ultraviolet-visible spectrum to vertical stimulus. The negative amounts of the chemical potential ( $\mu$ ) and the positive amounts of other parameters have observed a proper efficiency of TM (Fe, Ni, Zn)-doped graphene nanosheet for adsorption of CO.

Furthermore, TD-DFT/LANL2DZ, 6-31+G (d,p) calculations have been performed to assess the low lying stimulus states of CO adsorbed on the TM (Fe, Ni, Zn)-doped graphene nanosheets. The results contain the vertical stimulus energies, oscillator wavelengths, and strengths, which are shown in Figure 5a–c.

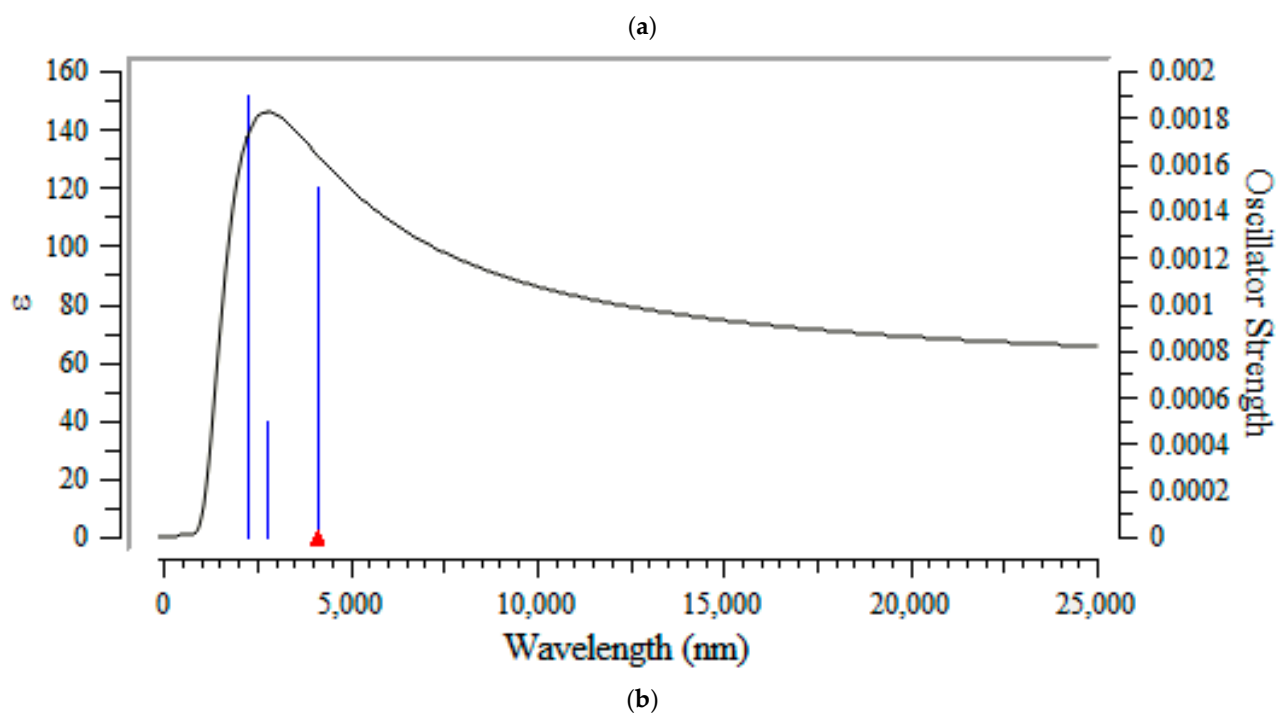
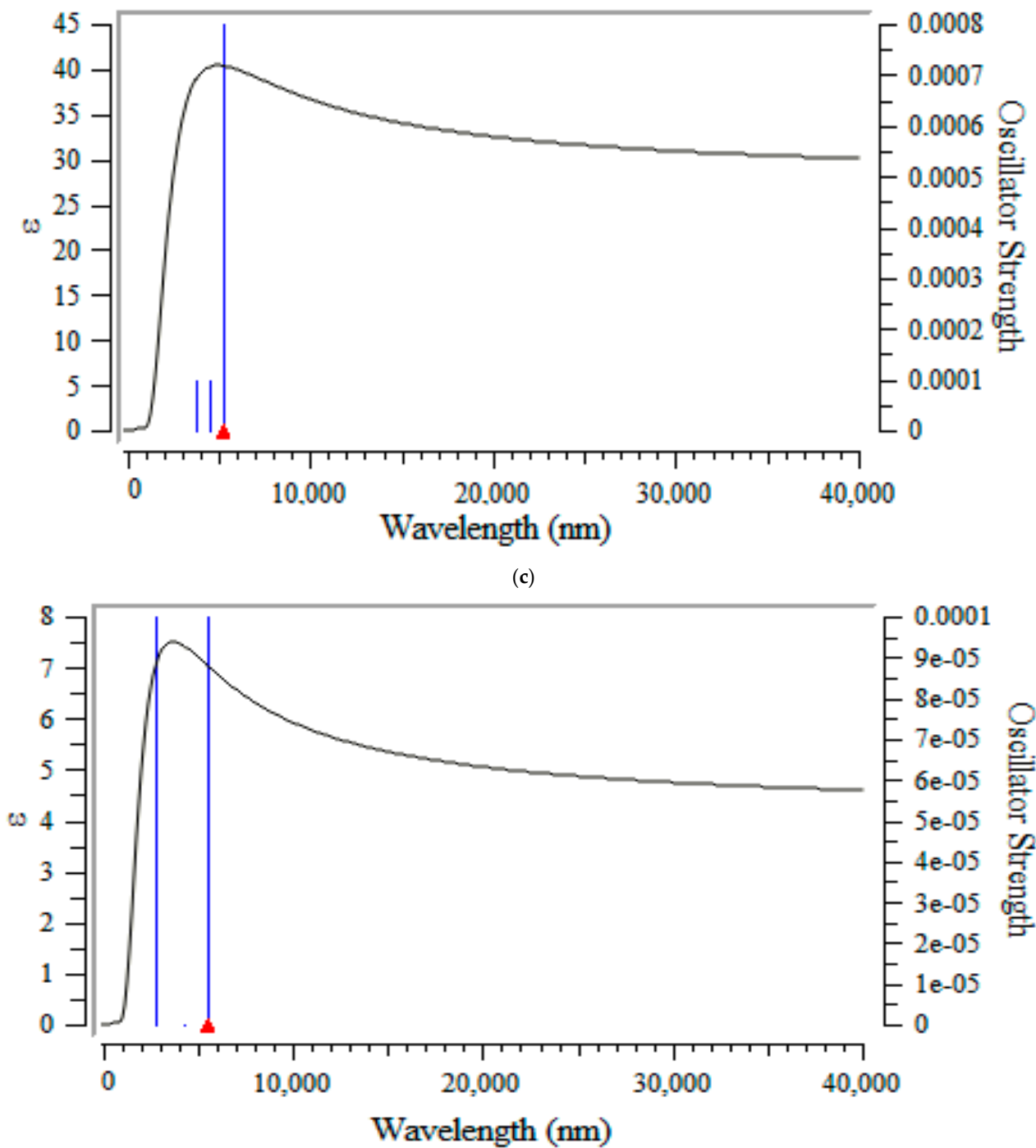


Figure 5. Cont.



**Figure 5.** UV-Vis spectra for (a) CO→ Fe-doped, (b) CO→ Ni-doped, and (c) CO→ Zn-doped on the graphene nanosheets.

Figure 5a–c show the UV-Vis spectra for CO→ Fe-doped, CO→ Ni-doped, CO→ Zn-doped graphene nanosheets, respectively, with maximum adsorption bands observed between 1000–5000 nm. Moreover, a sharp peak is observed around 4500 nm for CO→ Fe-doped, CO→ Fe-doped, and CO→ Fe-doped graphene nanosheets (Figure 5a–c).

#### 4. Conclusions

This article aimed to represent the study of the adsorption of the polluting gas carbon monoxide employing graphene nanosheets. The graphene nanosheets reviewed, in general physically adsorb many of the pollutant gas molecules considered, and these interactions can usually be enhanced by transition metal doping, which improves their detecting properties through chemisorption.

This work has reported the trends for carbon monoxide (CO) chemisorption on transition metal (iron, nickel, and zinc) doped graphene nanosheets.

In particular, the energetic, structural, and infrared adsorption characteristics of linearly (i.e., atop) adsorbed CO on (Fe, Ni, Zn)-doped graphene nanosheets have been discovered. Spin-unrestricted density functional theory (DFT) calculations were applied to predict the tendency of the CO adsorption energies (CO → Fe-doped, CO → Ni-doped, and CO → Zn-doped on the Gr nanosheets) and the C–O vibrational frequencies ( $\nu_{CO}$ ) for clusters composed of Fe, Ni, and Zn.

The effects of the transition metals' electronic structure on the adsorption energy of CO, and how these chemical factors might be related to the catalytic activity of transition metal catalysts that deal with the adsorption, and surface diffusion, have been investigated.

Finally, our research recommends that pristine graphene nanosheets can show physical adsorption of CO molecules, but after doping of GR nanosheets with the transition metals Fe, Ni, and Zn, the interaction between CO and the TM-doped graphene nanosheets has been directed toward a type of chemical adsorption. As a matter of fact, the sensitivity of TM-doped graphene nanosheets can be enhanced, making them good candidates for sensing CO gas.

**Author Contributions:** F.M.: Conceptualization and idea, Methodology, Software, Validation, Formal analysis, Investigation, Data Curation, Writing—original draft preparation, Visualization, Supervision, Project administration. M.M.: Methodology, Software, Formal analysis, Investigation, Data Curation, Writing—review and editing, Visualization, Resources. All authors have read and agreed to the published version of the manuscript.

**Funding:** This research received no external funding.

**Institutional Review Board Statement:** Not applicable.

**Informed Consent Statement:** All authors consent to participate in this research article.

**Data Availability Statement:** Not applicable.

**Acknowledgments:** In successfully completing this paper and its research, the authors are grateful to Kastamonu University for their support through the library, the laboratory, and scientific websites.

**Conflicts of Interest:** The authors declare no conflict of interest.

#### References

1. Mendes, P.C.D.; Ocampo-Restrepo, V.K.; Da Silva, J.L.F. Ab initio investigation of quantum size effects on the adsorption of CO<sub>2</sub>, CO, H<sub>2</sub>O, and H<sub>2</sub> on transition-metal particles. *Phys. Chem. Chem. Phys.* **2020**, *22*, 8998–9008.
2. Wang, M.; Zhang, B.; Ding, J.; Xu, N.; Bernards, M.T.; He, Y.; Shi, Y. Three-Dimensional Nitrogen-Doped Graphene Aerogel-Supported MnO Nanoparticles as Efficient Electrocatalysts for CO<sub>2</sub> Reduction to CO. *ACS Sustain. Chem. Eng.* **2020**, *8*, 4983–4994.
3. Ocampo-Restrepo, V.K.; Zibordi-Besse, L.; Da Silva, J.L.F. Ab initio investigation of the atomistic descriptors in the activation of small molecules on 3d transition-metal 13-atom clusters: The example of H<sub>2</sub>, CO, H<sub>2</sub>O, and CO<sub>2</sub>. *J. Chem. Phys.* **2019**, *151*, 214301. [[CrossRef](#)] [[PubMed](#)]
4. Montejo-Alvaro, F.; Martínez-Espinosa, J.A.; Rojas-Chávez, H.; Navarro-Ibarra, D.C.; Cruz-Martínez, H.; Medina, D.I. CO<sub>2</sub> Adsorption over 3d Transition-Metal Nanoclusters Supported on Pyridinic N<sub>3</sub>-Doped Graphene: A DFT Investigation. *Materials* **2022**, *15*, 6136. [[CrossRef](#)]
5. Cruz-Martínez, H.; Rojas-Chávez, H.; Montejo-Alvaro, F.; Peña-Castañeda, Y.; Matadamas-Ortiz, P.; Medina, D. Recent Developments in Graphene-Based Toxic Gas Sensors: A Theoretical Overview. *Sensors* **2021**, *21*, 1992. [[PubMed](#)]



6. Montejo-Alvaro, F.; González-Quijano, D.; Valmont-Pineda, J.A.; Rojas-Chávez, H.; Juárez-García, J.M.; Medina, D.I.; Cruz-Martínez, H. CO<sub>2</sub> Adsorption on PtCu Sub-Nanoclusters Deposited on Pyridinic N-Doped Graphene: A DFT Investigation. *Materials* **2021**, *14*, 7619.
7. Lisovski, O.; Piskunov, S.; Bocharov, D.; Zhukovskii, Y.F.; Kleperis, J.; Knoks, A.; Lesnicenoks, P. CO<sub>2</sub> and CH<sub>2</sub> Adsorption on Copper-Decorated Graphene: Predictions from First Principle Calculations. *Crystals* **2022**, *12*, 194. [[CrossRef](#)]
8. Ali, M.; Tit, N.; Yamani, Z.H. First principles study on the functionalization of graphene with Fe catalyst for the detection of CO<sub>2</sub>: Effect of catalyst clustering. *Appl. Surf. Sci.* **2020**, *502*, 144153. [[CrossRef](#)]
9. Salih, E.; Ayesh, A.I. Pt-doped armchair graphene nanoribbon as a promising gas sensor for CO and CO<sub>2</sub>: DFT study. *Phys. E Low-Dimens. Syst. Nanostruct.* **2021**, *125*, 114418. [[CrossRef](#)]
10. Kroto, H.W.; Heath, J.R.; O'Brien, S.C.; Curl, R.F.; Smalley, R.E. C<sub>60</sub>: Buckminsterfullerene. *Nature* **1985**, *318*, 162–163. [[CrossRef](#)]
11. Nasibulin, A.G.; Pikhitsa, P.V.; Jiang, H.; Brown, D.P.; Krashennikov, A.V.; Anisimov, A.S.; Queipo, P.; Moisala, A.; Gonzalez, D.; Lientschnig, G.; et al. A Novel Hybrid Carbon Material. *Nat. Nanotechnol.* **2007**, *2*, 156–161.
12. Moisala, A.; Nasibulin, A.G.; Shandakov, S.D.; Jiang, H.; Kauppinen, E.I. On-Line Detection of Single-Walled Carbon Nanotube Formation during Aerosol Synthesis Methods. *Carbon* **2005**, *43*, 2066–2074. [[CrossRef](#)]
13. Delgado, J.L.; Herranz, M.; Martín, N. The Nano-Forms of Carbon. *J. Mater. Chem.* **2008**, *18*, 1417. [[CrossRef](#)]
14. Falcao, E.H.; Wudl, F. Carbon Allotropes: Beyond Graphite and Diamond. *J. Chem. Technol. Biotechnol.* **2007**, *82*, 524–531.
15. Langenhorst, F.; Campione, M. Ideal and Real Structures of Different Forms of Carbon, with Some Remarks on Their Geological Significance. *J. Geol. Soc.* **2019**, *176*, 337–347. [[CrossRef](#)]
16. Zhou, Q.; Luo, S.; Xue, W.; Liao, N. Highly selective nitrogen dioxide gas sensing of ReS<sub>2</sub> nanosheets: A first-principles study. *Appl. Surf. Sci.* **2023**, *609*, 155388. [[CrossRef](#)]
17. Chen, M.; Yi, X.; Hu, X.; Zhou, X.; Tian, J.; Li, X. Correlation between the activity of Fe@ (N, S, and P) doped graphene catalysts and the coordination environment: A density functional theory study. *Int. J. Hydrog. Energy* **2023**, *48*, 171–179. [[CrossRef](#)]
18. Singla, M.; Sharma, D.; Jaggi, N. Effect of transition metal (Cu and Pt) doping/co-doping on hydrogen gas sensing capability of graphene: A DFT study. *Int. J. Hydrog. Energy* **2021**, *46*, 16188–16201. [[CrossRef](#)]
19. Joel, E.F.; Lujanienė, G. Progress in Graphene Oxide Hybrids for Environmental Applications. *Environments* **2022**, *9*, 153. [[CrossRef](#)]
20. Bijesh, P.; Selvaraj, V.; Andal, V. A review on synthesis and applications of nano metal Oxide/porous carbon composite. *Mater. Today Proc.* **2021**, *55*, 212–219.
21. Li, F.; Jiang, X.; Zhao, J.; Zhang, S. Graphene oxide: A promising nanomaterial for energy and environmental applications. *Nano Energy* **2015**, *16*, 488–515. [[CrossRef](#)]
22. El-Shazly, E.A.A.; Moussa, S.I.; Dakrouy, G.A. Recovery of Some Rare-Earth Elements by Sorption Technique onto Graphene Oxide. *J. Sustain. Met.* **2022**, *8*, 715–731. [[CrossRef](#)]
23. Su, Y.; Wang, J.; Wang, B.; Yang, T.; Yang, B.; Xie, G.; Zhou, Y.; Zhang, S.; Tai, H.; Cai, Z.; et al. Alveolus-inspired active membrane sensors for self-powered wearable chemical sensing and breath analysis. *ACS Nano* **2020**, *14*, 6067–6075. [[CrossRef](#)]
24. Ma, D.; Zhang, J.; Li, X.; He, C.; Lu, Z.; Lu, Z.; Lu, Z.; Yang, Z.; Wang, Y. C<sub>3</sub>N monolayers as promising candidates for NO<sub>2</sub> sensors. *Sens. Actuators B Chem.* **2018**, *266*, 664–673. [[CrossRef](#)]
25. Pacheco, M.; Pacheco, J.; Valdivia, R.; Santana, A.; Tu, X.; Mendoza, D.; Frias, H.; Medina, L.; Macias, J. Green Applications of Carbon Nanostructures Produced by Plasma Techniques. *MRS Adv.* **2017**, *2*, 2647–2659. [[CrossRef](#)]
26. Leenaerts, O.; Partoens, B.; Peeters, F.M. Adsorption of H<sub>2</sub>O, NH<sub>3</sub>, CO, NO<sub>2</sub>, and NO on graphene: A first-principles study. *Phys. Rev. B* **2008**, *77*, 125416. [[CrossRef](#)]
27. Bi, F.; Zhao, Z.; Yang, Y.; Gao, W.; Liu, N.; Huang, Y.; Zhang, X. Chlorine-Coordinated Pd Single Atom Enhanced the Chlorine Resistance for Volatile Organic Compound Degradation: Mechanism Study. *Environ. Sci. Technol.* **2022**, *56*, 17321–17330. [[CrossRef](#)]
28. Zhang, X.; Zhao, Z.; Zhao, S.; Xiang, S.; Gao, W.; Wang, L.; Xu, J.; Wang, Y. The promoting effect of alkali metal and H<sub>2</sub>O on Mn-MOF derivatives for toluene oxidation: A combined experimental and theoretical investigation. *J. Catal.* **2022**, *415*, 218–235. [[CrossRef](#)]
29. Wen, M.; Dong, F.; Yao, J.; Tang, Z.; Zhang, J. Pt nanoparticles confined in the ordered mesoporous CeO<sub>2</sub> as a highly efficient catalyst for the elimination of VOCs. *J. Catal.* **2022**, *412*, 42–58. [[CrossRef](#)]
30. Lee, S.W.; Lee, W.; Hong, Y.; Lee, G.; Yoon, D.S. Recent advances in carbon material-based NO<sub>2</sub> gas sensors. *Sens. Actuators B Chem.* **2018**, *255*, 1788–1804. [[CrossRef](#)]
31. Chatterjee, S.G.; Chatterjee, S.; Ray, A.K.; Chakraborty, A.K. Graphene-metal oxide nanohybrids for toxic gas sensor: A review. *Sens. Actuators B Chem.* **2015**, *221*, 1170–1181. [[CrossRef](#)]
32. Xiao, Z.; Kong, L.B.; Ruan, S.; Li, X.; Yu, S.; Li, X.; Jiang, Y.; Yao, Z.; Ye, S.; Wang, C.; et al. Recent development in nanocarbon materials for gas sensor applications. *Sens. Actuators B Chem.* **2018**, *274*, 235–267. [[CrossRef](#)]
33. Manna, A.K.; Pati, S.K. Tuning the electronic structure of graphene by molecular charge transfer: A computational study. *Chem.-Asian J.* **2009**, *4*, 855–860. [[CrossRef](#)]
34. Wang, W.; Zhang, Y.; Shen, C.; Chai, Y. Adsorption of CO molecules on doped graphene: A first-principles study. *AIP Adv.* **2016**, *6*, 025317. [[CrossRef](#)]

35. Boyd, A.; Dube, I.; Fedorov, G.; Paranjape, M.; Barbara, P. Gas Sensing Mechanism of Carbon Nanotubes: From Single Tubes to High-Density Networks. *Carbon* **2014**, *69*, 417–423.
36. Tabtimsai, C.; Keawwangchai, S.; Nunthaboot, N.; Ruangpornvisuti, V.; Wannoo, B. Density Functional Investigation of Hydrogen Gas Adsorption on Fe-doped Pristine and Stone-Wales Defected Single-walled Carbon Nanotubes. *J. Mol. Model.* **2012**, *18*, 3941–3949. [[CrossRef](#)]
37. Rather, S. Hydrogen Uptake of Ti-Decorated Multiwalled Carbon Nanotube Composites. *Int. J. Hydrogen Energy* **2021**, *46*, 17793–17801.
38. Zhang, X.; Dai, Z.; Wei, L.; Liang, N.; Wu, X. Theoretical Calculation of the Gas-Sensing Properties of Pt-Decorated Carbon Nanotubes. *Sensors* **2013**, *13*, 15159–15171. [[CrossRef](#)]
39. Zhang, X.; Dai, Z.; Chen, Q.; Tang, J. A DFT Study of SO<sub>2</sub> and H<sub>2</sub>S Gas Adsorption on Au-Doped Single-Walled Carbon Nanotubes. *Phys. Scr.* **2014**, *89*, 065803.
40. Hanaor, D.A.H.; Ghadiri, M.; Chrzanowski, W.; Gan, Y. Scalable Surface Area Characterization by Electrokinetic Analysis of Complex Anion Adsorption (PDF). *Langmuir* **2014**, *30*, 15143–15152. [[CrossRef](#)]
41. Mollaamin, F.; Shahriari, S.; Monajjemi, M.; Khalaj, Z. Nanocluster of Aluminum Lattice via Organic Inhibitors Coating: A Study of Freundlich Adsorption. *J. Clust. Sci.* **2022**, 1–16. [[CrossRef](#)]
42. Zhao, J.; Buldum, A.; Han, J.; Lu, J.P. Gas Molecule Adsorption in Carbon Nanotubes and Nanotube Bundles. *Nanotechnology* **2002**, *13*, 195–200. [[CrossRef](#)]
43. Stewart, J.J.P. Optimization of parameters for semiempirical methods I. Method. *J. Comput. Chem.* **1989**, *10*, 209–220. [[CrossRef](#)]
44. Svensson, M.; Humbel, S.; Froese, R.D.J.; Matsubara, T.; Sieber, S.; Morokuma, K. ONIOM: A Multilayered Integrated MO + MM Method for Geometry Optimizations and Single Point Energy Predictions. A Test for Diels–Alder Reactions and Pt(P(t-Bu)<sub>3</sub>)<sub>2</sub> + H<sub>2</sub> Oxidative Addition. *J. Phys. Chem.* **1996**, *100*, 19357–19363. [[CrossRef](#)]
45. Mollaamin, F. Features of parametric point nuclear magnetic resonance of metals implantation on boron nitride nanotube by density functional theory/electron paramagnetic resonance. *J. Comput. Theor. Nanosci.* **2014**, *11*, 2393–2398. [[CrossRef](#)]
46. Argaman, N.; Makov, G. Density functional theory: An introduction. *Am. J. Phys.* **2000**, *68*, 69. [[CrossRef](#)]
47. Chermette, H. Density functional theory: A powerful tool for theoretical studies in coordination chemistry. *Coord. Chem. Rev.* **1998**, *180*, 699.
48. Chermette, H.J. Chemical reactivity indexes in density functional theory. *Comput. Chem.* **1999**, *20*, 129.
49. Mollaamin, F.; Monajjemi, M. Molecular modelling framework of metal-organic clusters for conserving surfaces: Langmuir sorption through the TD-DFT/ONIOM approach. *Mol. Simul.* **2022**, 1–12. [[CrossRef](#)]
50. Ladeira, A.C.Q.; Ciminelli, V.S.T.; Duarte, H.A.; Alves, M.C.M.; Ramos, A.Y. Mechanism of anion retention from EXAFS and density functional calculations: Arsenic (V) adsorbed on gibbsite. *Geochim. Cosmochim. Acta* **2001**, *65*, 1211.
51. Sousa, S.F.; Fernandes, P.A.; Ramos, M.J. General performance of density functionals. *J. Phys. Chem. A* **2007**, *111*, 10439. [[CrossRef](#)]
52. Koch, W.; Holthausen, M.C. *A Chemist's Guide to Density Functional Theory*; Wiley-VCH: New York, NY, USA, 2001.
53. Hohenberg, P.; Kohn, W. Inhomogeneous Electron Gas. *Phys. Rev. B* **1964**, *136*, B864–B871. [[CrossRef](#)]
54. Kohn, W.; Sham, L.J. Self-Consistent Equations Including Exchange and Correlation Effects. *Phys. Rev.* **1965**, *140*, A1133–A1138.
55. Becke, A.D. Density-functional thermochemistry. III. The role of exact exchange. *J. Chem. Phys.* **1993**, *98*, 5648–5652.
56. Lee, C.; Yang, W.; Parr, R.G. Development of the Colle–Salvetti correlation-energy formula into a functional of the electron density. *Phys. Rev. B* **1988**, *37*, 785–789. [[CrossRef](#)]
57. Kim, K.; Jordan, K.D. Comparison of Density Functional and MP2 Calculations on the Water Monomer and Dimer. *J. Phys. Chem.* **1994**, *98*, 10089–10094. [[CrossRef](#)]
58. Stephens, P.J.; Devlin, F.J.; Chabalowski, C.F.; Frisch, M.J. Ab Initio Calculation of Vibrational Absorption and Circular Dichroism Spectra Using Density Functional Force Fields. *J. Phys. Chem.* **1994**, *98*, 11623–11627. [[CrossRef](#)]
59. Cramer, C.J. *Essentials of Computational Chemistry: Theories and Models*, 2nd ed.; Wiley: Hoboken, NJ, USA, 2004.
60. Vosko, S.H.; Wilk, L.; Nusair, M. Accurate spin-dependent electron liquid correlation energies for local spin density calculations: A critical analysis. *Can. J. Phys.* **1980**, *58*, 1200–1211. [[CrossRef](#)]
61. Becke, A.D. Density-functional exchange-energy approximation with correct asymptotic behavior. *Phys. Rev. A* **1988**, *38*, 3098–3100.
62. Ditchfield, R.; Hehre, W.J.; Pople, J.A. Self-consistent molecular-orbital methods. IX. An extended Gaussian-type basis for molecular-orbital studies of organic molecules. *J. Chem. Phys.* **1971**, *54*, 724–728. [[CrossRef](#)]
63. Frisch, M.J.; Trucks, G.W.; Schlegel, H.B.; Scuseria, G.E.; Robb, M.A.; Cheeseman, J.R.; Scalmani, G.; Barone, V.; Petersson, G.A.; Nakatsuji, H.; et al. *Gaussian 16, Revision C.01*; Gaussian, Inc.: Wallingford, CT, USA, 2016.
64. Fry, R.A.; Kwon, K.D.; Komarneni, S.; Kubicki, J.D.; Mueller, K.T. Solid-State NMR and Computational Chemistry Study of Mononucleotides Adsorbed to Alumina. *Langmuir* **2006**, *22*, 9281–9286. [[CrossRef](#)]
65. Kohn, W.; Becke, A.D.; Parr, R.G. Density Functional Theory of Electronic Structure. *J. Phys. Chem.* **1996**, *100*, 12974–12980. [[CrossRef](#)]
66. Parr, R.G.; Pearson, R.G. Absolute Hardness: Companion Parameter to Absolute Electronegativity. *J. Am. Chem. Soc.* **1983**, *105*, 7512–7516. [[CrossRef](#)]
67. Politzer, P.; Abu-Awwad, F. A comparative analysis of Hartree-Fock and Kohn-Sham orbital energies. *Theor. Chem. Acc.* **1998**, *99*, 83–87. [[CrossRef](#)]

- 
68. Aihara, J. Reduced HOMO–LUMO Gap as an Index of Kinetic Stability for Polycyclic Aromatic Hydrocarbons. *J. Phys. Chem. A* **1999**, *103*, 7487–7495. [[CrossRef](#)]
  69. Silverstein, R.M.; Bassler, G.C.; Morrill, T.C. *Spectrometric Identification of Organic Compounds*, 5th ed.; John Wiley & Sons, Inc.: New York, NY, USA, 1981.

**Disclaimer/Publisher’s Note:** The statements, opinions and data contained in all publications are solely those of the individual author(s) and contributor(s) and not of MDPI and/or the editor(s). MDPI and/or the editor(s) disclaim responsibility for any injury to people or property resulting from any ideas, methods, instructions or products referred to in the content.